Status Update: Cavity-Enhanced Thomson Scattering for Electron Measurements in Electric Propulsion Devices

IEPC-2017-279

Presented at the 35th International Electric Propulsion Conference
Georgia Institute of Technology • Atlanta, Georgia • USA
October 8 – 12, 2017

Adam J. Friss[1] and Azer P. Yalin[2]
Colorado State University, Fort Collins, CO, 80523, USA

We report on the current status of the Cavity Enhanced Thomson Scattering (CETS) diagnostic relative to previous work. The instrument has progressed from a low-power proof of concept to a high-power system integrated to vacuum facilities. High-power cavity locking has been demonstrated in laboratory air resulting in intra-cavity powers of 3.2 kW and a build-up factor of 3300. Rotational Raman and Rayleigh scattering measurements have been made over relatively short collection times demonstrating the ability of the technique to detect weak scattering signals. Locking in the vacuum chamber and in the presence of plasma has proven challenging but has been demonstrated over short time periods (<1 min). The system servo bandwidth and frequency noise have been characterized and steps to improve the locking and enable plasma measurements have been identified.

Nomenclature

AOM	=	acousto-optic modulator
BaO	=	barium oxide
CETS	=	cavity enhanced Thomson scattering
CW	=	continuous-wave
EEDF	=	electron energy distribution function
EOM	=	electro-optic modulator
EP	=	electric propulsion
HR	=	high reflectivity
I_{cav}	=	intra-cavity power
I_L	=	power of source laser
LTS	=	laser Thomson scattering
n_e	=	electron number density
NIR	=	near infrared
PBS	=	polarizing beam splitter
PD	=	photodiode
PDH	=	Pound-Drever-Hall
PMT	=	photomultiplier tube
PZT	=	piezo actuator
R	=	cavity mirror reflectivity
ROC	=	radius of curvature
$\mathrm{T_e}$	=	electron temperature
σ_{Th}	=	Thomson scattering cross section
$\delta\nu_{\mathrm{cavity}}$	=	cavity linewidth
$\delta\nu_{\mathrm{laser}}$	=	laser linewidth

[1] Graduate Student, Department of Mechanical Engineering, ajf787@rams.colostate.edu.
[2] Professor, Department of Mechanical Engineering, ayalin@engr.colostate.edu.

I. Introduction

ELECTRON property measurements are crucial for the development and experimental testing of electric propulsion systems, as well as for the validation of numeric models. Measurements of electron density (n_e) and electron energy distribution function (EEDF) can be made with physical probes, e.g. Langmuir probes, or optically with the use of laser Thomson scattering (LTS). Physical probe measurements have been an indispensable tool of the EP community and have been used extensively for nearly a century[1]. However, probe measurements can be challenging within the thruster channel and may affect thruster operation and result in unwanted plasma perturbations[2,3]. LTS measurements are appealing due to the non-perturbing nature of the technique, but suffer from low signal levels and optical interference[4–6], making application to EP systems very challenging[7].

Laser Thomson measurements of EP systems are very difficult due to the small scattering cross section[4] (integrated cross-section of σ_{Th}=6.65×10^{-29} m^2) and low plasma density (~10^9 - 10^{15} cm^{-3})[8], which make detection of scattered signals in the presence of much stronger Rayleigh and/or elastic scattered light signals (spectrally positioned at the center of the LTS lineshape) very difficult[4–6]. Typical experiments employ relatively high power pulsed lasers, e.g. Q-switched Nd:YAG lasers with pulse energies of ~0.1-1 J and repetition rates of ~10-100 Hz (average power of ~1-100 W)[5,6,9–13], in order to obtain usable signal levels. Given these challenges, measurements at a single plasma condition in a weakly ionized discharge are very difficult and often require tens of minutes, or more, with detection limits of n_e ~10^{10}-10^{12} cm^{-3} being considered state-of-the-art[5]. The technique we are developing, termed cavity-enhanced Thomson scattering (CETS), uses the same spectroscopic approach as conventional LTS, but relies upon a high-power CW beam generated in an optical build-up cavity to increase the scattered photon counts and signal levels. The build-up cavity is based upon frequency locking a high-power narrow-linewidth laser to a high-finesse cavity (or vice versa), which results in an intra-cavity beam power as high as ~10-100 kW. Although the average power is much higher, the peak power is much lower, which may be advantageous in reducing plasma perturbations[14] though introduces challenges in detection since time-gating around the laser pulse (to reduce collection of background emission) can no longer be done in the traditional way.

Further details of the diagnostic approach are presented in Section II. Low- and high-power CETS experimental setup and results, details of the bench-top vacuum facility and cathode, plasma locking results, and system noise characterization are presented in section III. Locking limitations and approach as well as expected outcomes are presented in section IV. Finally, conclusions are presented in section V.

II. Diagnostic Approach

A. Theory

The CETS diagnostic technique has been discussed extensively in past publications[15–18], but a brief overview is presented here. A high-finesse optical cavity is formed from two dielectric coated mirrors with reflectivity R >0.999. A near-infrared (NIR) narrow-linewidth ytterbium fiber laser at 1064 nm is frequency locked to the optical cavity using the Pound-Drever-Hall locking technique[19], which results in a large buildup of intra-cavity power. The cavity is integrated around the EP device under test such that the plasma overlaps the intra-cavity beam. The Thomson scattered light from the high-power intra-cavity beam is collected by a lens and then relayed to a triple-monochromator for dispersion (and elastic background suppression). Finally, the signal is detected with a photomultiplier tube (PMT) and multichannel scaler for photon counting. The monochromator is scanned in wavelength to measure the Thomson line shape, which allows determination of electron properties.

The intra-cavity power is a function of the mirror reflectivity, incident laser power, and cavity coupling. The cavity enhancement or build-up factor, defined as I_{cav}/I_L, increases with mirror reflectivity while the width of the cavity transmission peak narrows. Therefore, to take full advantage of the large build-up factors achievable with high reflectivity mirrors, efficient coupling in the frequency domain most be achieved ,which requires the use of a narrow line-width source such that $\delta\nu_{laser} \leq \delta\nu_{cavity}$. Coupling of the laser to the cavity in the spatial domain[20] is also important for power coupling and cavity mode operation (TEM_{00}). If the laser were perfectly matched to the cavity in the spatial and frequency domains, the coupling factor would approach unity. In such cases, the cavity build-up factor approaches 2/(1-*R*) allowing, for example, enhancements of 200,000 for mirrors with *R*=0.99999. Operation in the NIR is advantageous because the ratio of Thomson to competing Rayleigh scattering cross-sections is improved, plasma emission is reduced, and narrow-linewidth high-power fiber laser sources are readily available. However, photodetectors typically have lower quantum efficiency in the NIR relative to visible or ultraviolet wavelengths (e.g. QE ~0.40 at 532 nm versus ~0.025 at 1064nm). Additionally, care must be taken to reduce or eliminate background sources of NIR radiation in the field of view of the collection optics, such as black body radiation or plasma emission.

III. Experimental Setup and Results

A. Low-Power CETS Setup

The initial development of the CETS instrument (Fig. 1) was accomplished using a single-mode narrow-linewidth (<5 kHz) fiber laser (SI-2000, Continuum) operating at 1064 nm with an output power of ~20 mW. A fiber based optical isolator was used to prevent reflected light from propagating back into the laser, which can cause wavelength instabilities and, in some cases, damage to the laser gain medium. The fiber output was coupled to an aspheric collimation lens and then passed through a bandpass filter centered at 1064 nm to remove residual 980 nm pump light present in the laser output. The polarization of the beam was rotated via a half wave plate (λ/2) to optimize transmission through a polarizing beam splitter (PBS). An acousto-optic modulator (AOM), quarter wave plate (λ/4), lens, and mirror were used in a cat's eye[21] (double-pass) configuration to rapidly modulate the frequency of the beam, which provides a means to combat high frequency noise during cavity locking. During an earlier iteration of the CETS instrument, frequency locking of the laser to the cavity was performed using only a piezo actuator on the first cavity mirror. The piezo bandwidth was not sufficient to maintain a high-quality lock so the double-pass AOM was implemented as a means to provide fast feedback, while the mirror piezo was used to combat slow sources of noise (e.g. thermal drift, low frequency vibrations, pressure fluctuations, etc.).

Mode-matching of the beam to the cavity was performed with the use of a lens (MM lens) mounted on a translation stage at the PBS output. A half wave plate and polarizer were used to rotate the beam polarization to match the electro-optic modulator (EOM) and PBS. The EOM (Photonics Technologies, EOM-01-12.5-IR) was used to generate laser side bands at ± 12.5 MHz for PDH locking. The PBS, quarter wave plate, mirror, lens, and photodiode (PD) were used to pick out the light reflected from the first cavity mirror (M1) to generate the locking error signal. The optical cavity was 50 cm in length and formed with two HR mirrors. The cavity was constructed of brass tubing and KF vacuum hardware and was designed to operate from vacuum to ambient pressure with a variety of gases. The first cavity mirror had an infinite radius of curvature (flat) and was mounted in a custom mirror holder that contained a piezo-actuator (PZT) used for modulation of the cavity length. The second cavity mirror (M2) had a radius of curvature (ROC) of 1 m. The cavity pressure and temperature were monitored via a pressure transducer (PT) and thermocouple (TC), respectively.

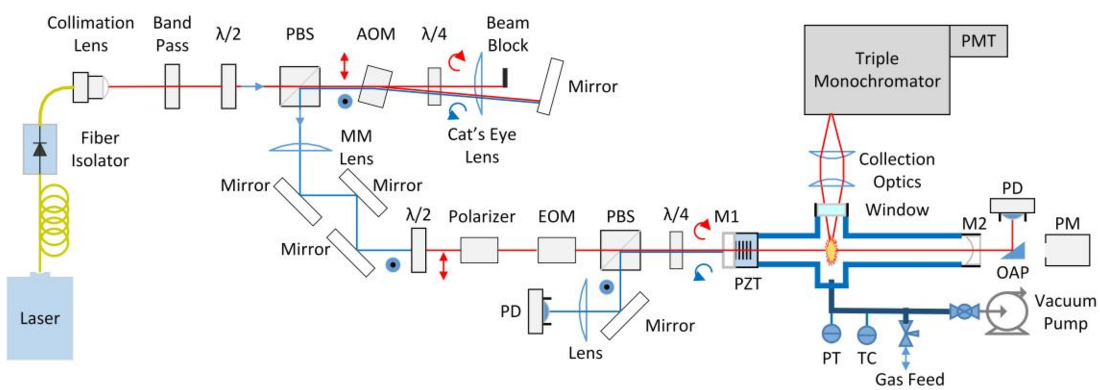

Figure 1. Schematic diagram of the low-power CETS scattering setup. *A high-finesse optical cavity is frequency locked to a narrow-linewidth laser source using the Pound-Drever-Hall technique. The cavity lock is maintained via feedback to the cavity mirror piezo actuator (PZT) and double-pass AOM. Polarization is show by red and blue arrows. Beams have been offset and angles exaggerated for clarity.*

Scattering signals were collected through a 2.5 cm diameter window via a pair of 200 mm focal length relay lenses and coupled into the entrance slit of a triple-monochromator (SPEX-1877) using two 2-inch steering mirrors (not shown in Fig. 1). The first stage of the SPEX, formed of a double monochromator in subtractive dispersion mode, acted as a wavelength-selectable bandpass filter. The final stage of the SPEX, known as the spectrograph stage, dispersed the light over the exit slit, which was coupled to a near-infrared photomultiplier tube (Hamamatsu, H10330B). The PMT signal was monitored with a multichannel scaler (Stanford Research Systems, SR430) for photon counting.

B. Low-Power Rotational Raman Scattering Measurements

As a proof of concept demonstration rotational Raman and Rayleigh scattering data was collected using the experimental setup described in section IIIA. The cavity was evacuated using a vacuum pump and then charged with pure nitrogen (Fig. 2a), oxygen (Fig. 2b), and carbon dioxide (Fig. 2c). The intra-cavity power was 22 W based on a measured (via cavity ring-down) mirror reflectivity (R) of 0.99985 and incident laser power of 3.7 mW. The data is plotted along with a synthetic spectrum calculated using know rotational constants and measured system parameters. The rotational Raman and Rayleigh scattering model is presented in detail in an earlier publication[22]. The data was collected at 0.001 nm increments and was normalized by the transmitted cavity power to remove intra-cavity power fluctuations, which manifest as noise in the data. The synthetic spectra for nitrogen, oxygen, and carbon dioxide were scaled by 1.50, 1.87, and 1.15 respectively. The discrepancy between the model and the actual data arises from the difficulty in quantifying the total system efficiency and due to higher order TEM mode operation, which adds error to the intra-cavity beam size calculation. The scattering measurements served to demonstrate the ability of the CETS technique to collect very weak scattering phenomena.

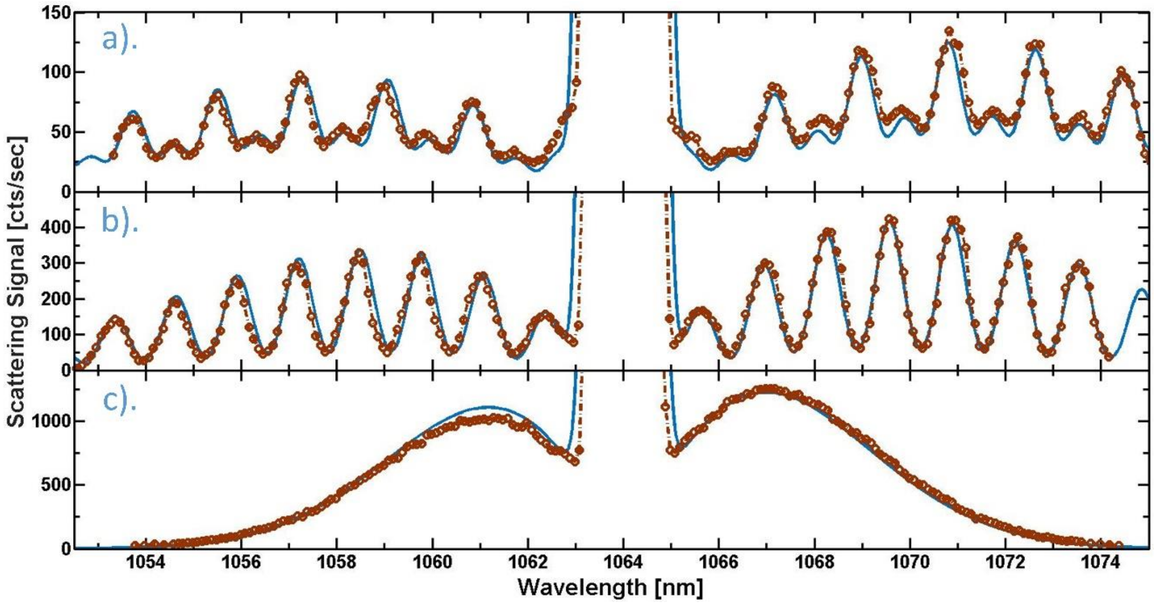

Figure 2. Rotational Raman and Rayleigh scattering in gasses. *Experimental scattering data (red circles and dashed line) and synthetic spectra (blue line) are presented for a). Nitrogen, b). Oxygen, and c). Carbon dioxide.*

C. High-Power CETS Setup

After successful demonstration of the CETS technique using a low-power laser source, the system was re-designed to incorporate a high-power 5.4 W fiber laser (NP Photonics, RFLSA-5000-3-1064-PM-SA1). In addition to a new laser source the isolator and EOM were replaced with high damage threshold photonics, the double-pass AOM setup was changed, and the polarization optics used to pick the reflected cavity beam out of the beamline for generation of the PDH error signal was removed. The high-power experimental setup is presented in figure 3 below.

Due to the alignment difficulty and unacceptable beam steering the double pass “cat’s eye” configuration was abandoned and instead a simpler configuration with a convex mirror is now used. The beam is focused to a waist using a lens and the AOM is centered at the waist location. The mirror is positioned a distance away from the beam waist location equal to its ROC (20 cm). All incoming rays from the AOM are retroreflected independent of angle of incidence and therefore modulation frequency. To guarantee the retroreflected beam does not diverge, a focusing lens should be selected such that the beam ROC matches the mirror ROC at the mirror location. The double pass setup simplified the alignment procedure and reduced beam steering over the frequency range of interest (6.3 μrad in this case versus 116 μrad with the cat’s eye).

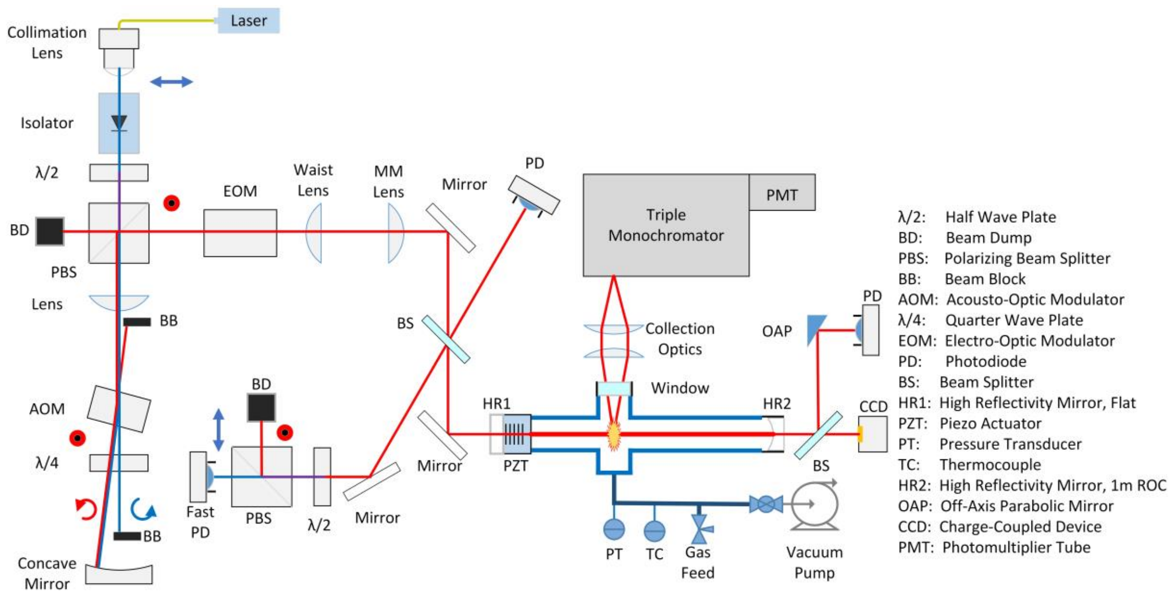

Figure 3. Schematic diagram of the high-power CETS setup. *A high-finesse optical cavity is frequency locked to a narrow-linewidth laser source. Polarization is shown by red and blue arrows. Beam offsets have been exaggerated for clarity.*

The use of polarization optics to sample the beam reflected from the first cavity mirror in the low-power instrument required circularly polarized light incident (and within) the cavity, which created an intra-cavity standing wave with a polarization vector constant in time but rotated in space along the cavity axis (z-direction). The standing wave formed in the cavity can be decomposed into two beams with orthogonal linear polarization along the x- and y- directions which, given the dependence of Thomson scattering on polarization and collection angle[4,23], reduced the collected signal by a factor of two. Therefore, by using a purely linearly polarized intra-cavity beam the collected scattering signal can be doubled. A thin film beam splitter was instead used and allowed for linearly polarized light within the cavity as well as a reduction in the reflected power incident on the photodiode, which otherwise would have saturated and possibly damaged the diode.

D. High-Power CETS Locking and Scattering

After integration of the high-power laser and associated modifications, the cavity coupling, lock quality, and scattering signal were monitored at various laser power settings and compared with earlier low-power work. The low-power setup coupling factor was found to be C~0.15 to 0.25, while the high-power setup demonstrated an average coupling of C= 0.20. The lock quality can be characterized from the amplitude of the error signal and the ability to maintain the lock in the presence of large transient perturbations (e.g. acoustic noise, pump cycling, personnel movement in lab, etc.). The error signal is a measure of the systems deviation from the set point, which for the CETS diagnostic is the resonant condition. A large amplitude in the error signal indicates the laser and cavity are far from the resonant condition. A low-quality lock is a result of poor servo loop optimization and/or the presence of frequency noise (drift) that exceeds the bandwidth of the servo loops. The high-power setup required new PID tuning parameters for the two servo loops but demonstrated comparable error signal amplitudes (10's of mV). Additionally, a study of scattering signal strength as a function of incident laser power was performed by detecting rotational Raman scattering in laboratory air at a wavelength of approximately 1070.8 nm. The laser power was gradually increased while the cavity coupling, lock quality, and scattering signal strength were monitored. The measured parameters were constant over the full power range of the study and the scattering signal amplitude followed a linear trend. The maximum intra-cavity power was 3.2 kW. As the system performance is improved, much higher intra-cavity powers will be present.

Rotational Raman spectra (Fig. 4) were again measured to further verify high-power system performance and to calibrate the collection system in both wavelength and signal amplitude. The measurements were performed in laboratory air at atmospheric pressure (0.85 atm), an intra-cavity power of 3.2 kW, and with a collection time of 20.97 seconds (black x's) and 5.12 milliseconds (red circles) per data point. Despite four orders of magnitude reduction in sampling time, the two data sets are in excellent agreement with each other and the simulation (blue line). As the coupling of the CETS system and/or the mirror reflectivity is increased the collection time required to resolve high-quality spectra will be further reduced, which is useful for measuring transient phenomena.

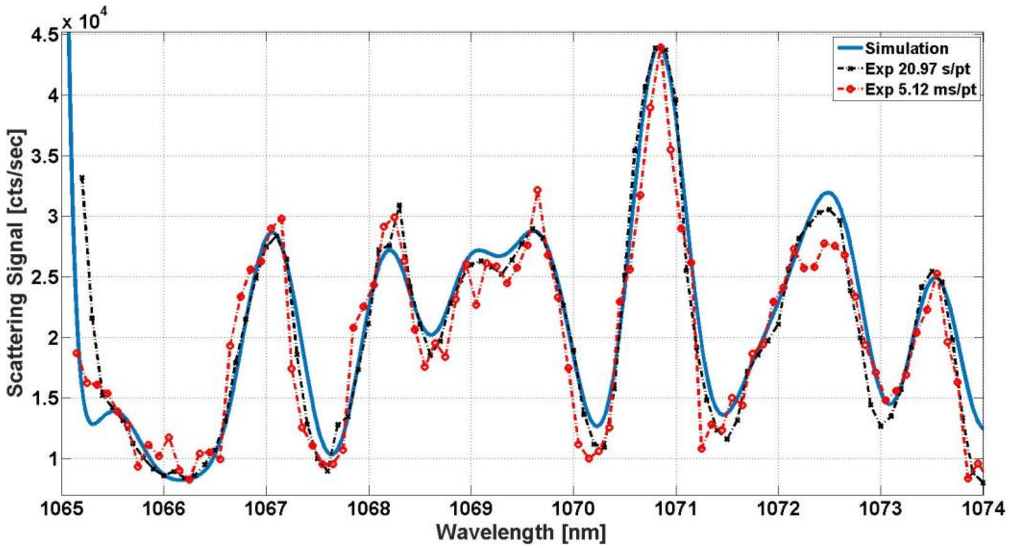

Figure 4. Rotational Raman scattering in laboratory air. *The synthetic spectra of room air (78.09% N_2, 20.95% O_2, and 0.04% CO_2) is shown as a solid blue line. Experimental scattering data is presented for a collection time of 20.97 seconds per point (black x's and dashed line) and 5.12 milliseconds per point (red circles and a dashed line). The data points close to 1074 nm have been artificially diminished in amplitude due to proximity to the edge of the monochromator bandpass of the filter stage.*

E. Vacuum Facility and Hollow Cathode Operation

A bench-top 50-cm spherical vacuum chamber (Fig. 5a) is used for initial plasma studies. The chamber is equipped with a residual gas analyzer, ion gauge, gas and electrical feed throughs, and a turbo molecular pump. The chamber can reach a base pressure of 9 μTorr and maintains a pressure of 520 μTorr during cathode operation for a propellant flow rate of 7.5 sccm. The optical cavity is formed from two HR mirrors attached to the chamber via QF flanges. Due to the chamber dimensions and height above the beamline, a periscope was added and the length of the cavity was changed to 85 cm. A complete cavity alignment as well as a new mode match was implemented and confirmed by locking the cavity and observing the transmitted beam mode with a CCD.

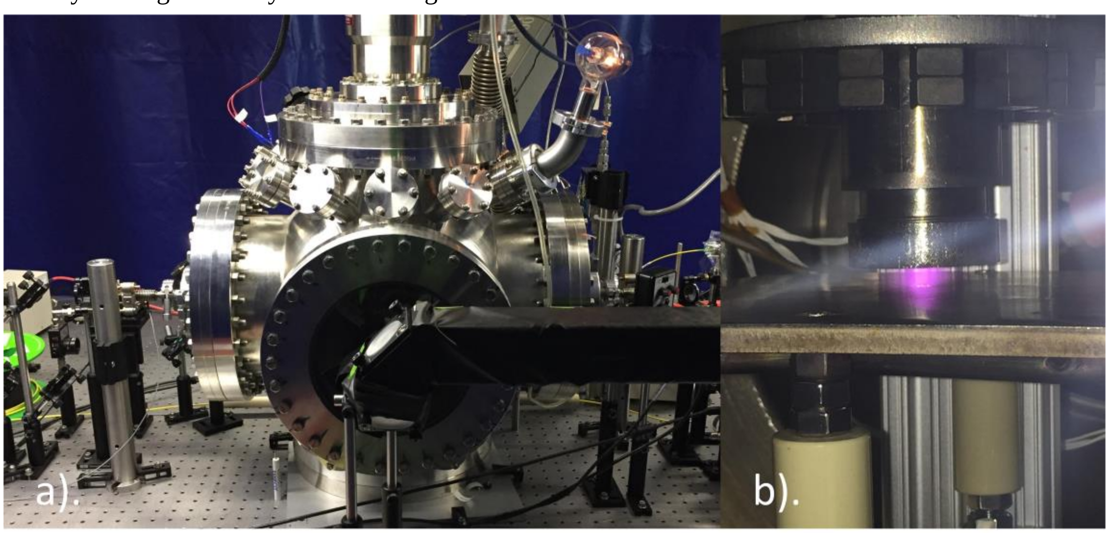

Figure 5. Bench-top vacuum facility and cathode. *a). The vacuum facility serves as a test bed for initial CETS plasma measurements in the plume of a hollow cathode. b). BaO hollow cathode with water cooled plate anode and axial magnetic field.*

An instant-start hollow cathode from Plasma Controls LLC. with a barium oxide (BaO) based tungsten ceramic composite insert is used for initial CETS testing (Fig. 5b). A water cooled plate anode is used to reduce unwanted black body radiation due to heating and for ease of cathode coupling. An axial magnetic field is generated with a circular array of permanent rare earth magnets. The cathode is currently operated on argon but can be switched to xenon propellant for Thomson scattering studies. The cavity beam is aligned directly below the cathode orifice plate and the collection optics gather the scattered light through the large chamber window (Fig. 5a). Optimization of the collection system is accomplished by flowing nitrogen through the cathode while under vacuum and measuring the rotation Raman scattering signal strength (since actual atomic propellant species do not have Raman spectra). Because the gas density and scattering signals are largest directly below the orifice plate outlet, the system can be readily aligned to target regions of high electron density for the operating cathode

F. Laser Locking in Presence of Plasma and Frequency Noise

Initial plasma locking studies have been performed with the cathode operating on argon. The cavity was locked and scattering data was collected at several wavelengths. The data did not show a clear Thomson signal contribution, due to a combination of large background (elastic) signals, poor coupling, and low plasma density. The cavity coupling was $C<0.01$ and the lock was unstable. The transmitted cavity signal can be used to monitor intra-cavity power and diagnose the locking (figure 6b below). There is nominally more transmitted cavity power when the laser is locked, but when compared to the cavity transmission from the gas scattering cavity (Fig. 6a) described in sec. IIIA it is clear the system performance has been significantly reduced. After re-tuning the PID controllers, and an extensive locking investigation, it was determined that the cavity mirror piezo had insufficient bandwidth to combat the new noise sources, and so the locking scheme was reconfigured to provide feedback to the laser piezo element instead of the cavity piezo. The laser piezo provides ~300 MHz of tuning at a bandwidth up to 10 kHz whereas the cavity piezo provides several GHz of tuning, but at only a bandwidth of several hundred Hz. Additionally, the cavity piezo is in physical contact with the mirror surface and depending on how tight the mirror is secured in the holder the piezo experiences a different preload force, which results in a change in tuning response. Therefore, tuning of the PID controller was required anytime the mirror was removed for cleaning. The laser tuning resulted in an improved lock quality and coupling (Fig. 6c) but overall was still lower than the previous system. The coupling was found to be $C\sim0.03$ but the ability to maintain the lock was reduced from several minutes to 20-40 seconds.

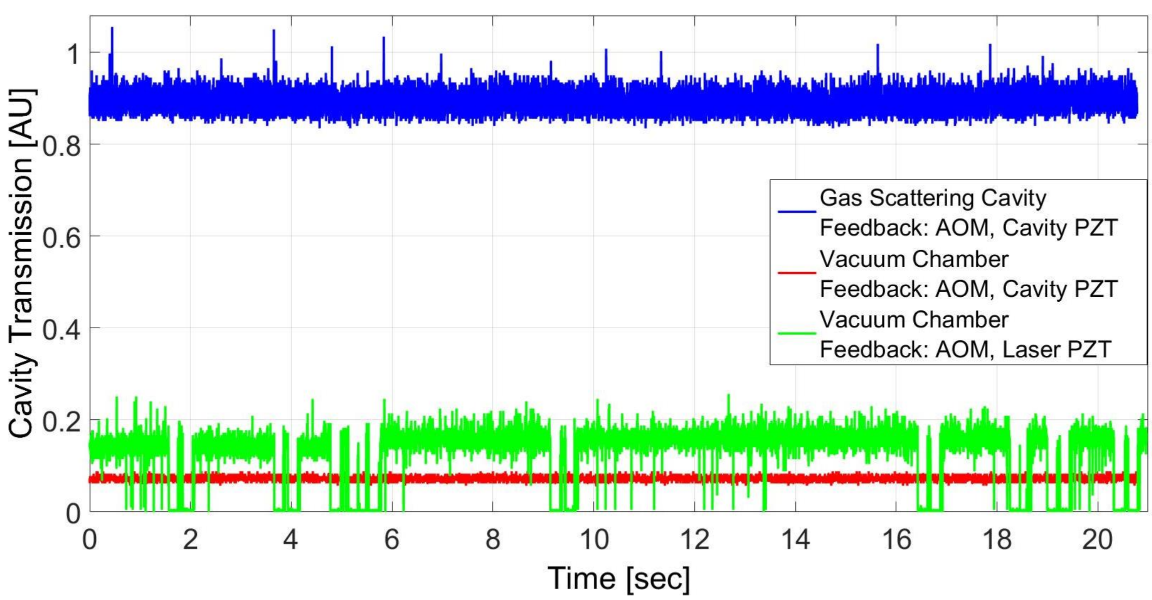

Figure 6. High-power cavity locking comparison. *The locked cavity transmission signal for the gas scattering cavity design (blue), vacuum chamber with cavity piezo (red), and vacuum chamber with laser piezo (green) are compared.*

A study of the system frequency noise was performed to determine noise sources and to inform strategies to improve the locking. The laser frequency was scanned over a cavity transmission peak using a triangle wave form and the transmitted signal monitored with a photodiode. By tracking the frequency position of the cavity peak (as measured by the laser) one gains information on the temporal nature of their relative positions – from which one can determine the frequency extent (shift) and associated bandwidth required for locking. A 10 MHz oscilloscope was used to collect several hundred scan wave forms of the ramp signal and cavity transmission. By looking at the position of the transmission peak with respect the scan signal one can track the extent of the system perturbation. Additionally, by varying the scan signal frequency it was possible to sample the cavity noise via the peak transmission signal at frequencies up to 2 kHz. Only data from the up-ramp scan was used for the study to avoid any additional noise introduction due to piezo hysteresis. The position of the transmission peak in time for the vacuum facility with none of the equipment running and with all the pumps (roughing and turbo) and the plasma source operational is shown in figure 7. There is significantly more noise on the system when the vacuum facility is operational, as would be expected.

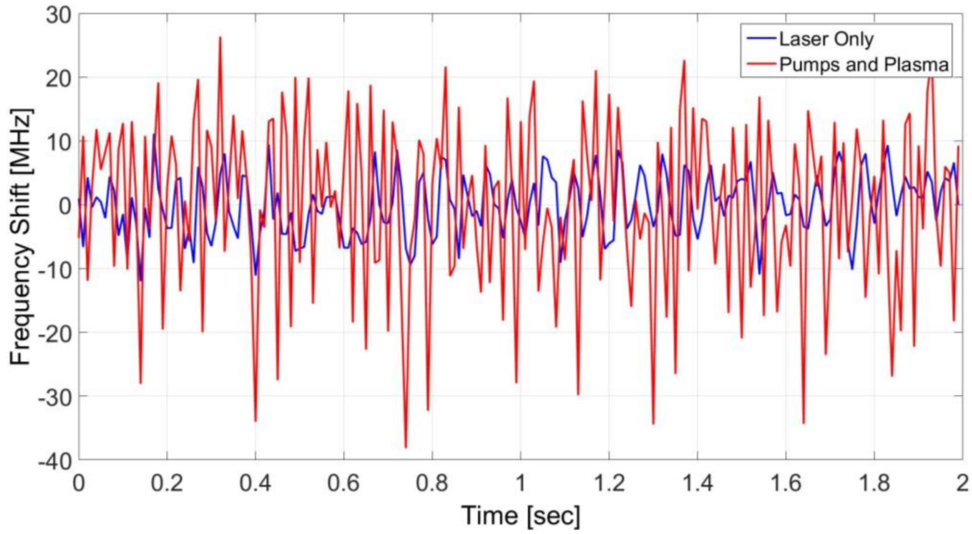

Figure 7. Transmission peak position. *The laser frequency was scanned over a cavity transmission peak at a rate of 100 Hz and the peak position was recorded.*

Further studies were performed tracking the peak position in time with various pieces of equipment running to determine major sources of frequency noise. The maximum extent (shift) from the mean value, along with its standard deviation, and peak frequency were determined and are presented in table 1 (for a 500 Hz laser scan rate). Peak frequency refers to the frequency having the maximum contribution of the power spectral density of the shifts (as found from PSD of the time-dependent shift data). Unsurprisingly, low frequency contributions were present in the frequency noise, as well as contributions at 60 Hz and its harmonics due to reciprocating pumps. The low frequency noise is likely due to thermal and pressure variations of the room and low frequency vibrations. It is likely the turbomolecular pump is adding significant mechanical vibrations at very high frequencies but due to a limitation in laser scan speed it is not possible to resolve noise beyond ~ 1 kHz.

Operational Equipment	Max Extent from Mean [MHz]	Extent Standard Deviation [MHz]	Peak Frequency [Hz]
Laser	15.5	6.1	20.0
Laser /Rough Pump	34.4	12.6	57.5
Laser/Rough Pump/Turbo Pump	38.0	15.2	235.0
Laser /Rough Pump/ Turbo Pump / Plasma	37.4	13.3	235.0

Table 1. Frequency noise Characteristics of main equipment.

IV. Next Steps

A. Locking Limitations and Control Approach

The available forms of feedback and their characteristics are presented in table 2. Based on the current noise data, the available feedback methods should be sufficient to lock the cavity. The implementation of the locking (for example filters and software details) must be re-examined to fully capitalize on available shift extent and bandwidth.

Form of Feedback	Extent [MHz]	Bandwidth [kHz]
Cavity Piezo	~3440	<1
Laser Piezo	300	10
Double Pass AOM	44	20,000

Table 2. System Feedback.

Further system improvements will include a re-design of the optical cavity for improved vibration isolation of the vacuum equipment. Currently, the optical cavity is directly coupled to the chamber body with the mirrors themselves forming part of the vacuum boundary. In such a configuration, any mechanical vibrations are transferred to the mirrors. Instead, we intend to implement a modular framework to house the cavity itself inside the chamber on its own support structure. The setup will be relatively similar to optical cavities we have developed for cavity ring-down spectroscopy studies of thruster erosion[24] and is expected to be significantly more robust against frequency noise. By displacing the thruster (or cathode) relative to the cavity, it will be possible to probe various positions.

B. CETS Spectral Simulations

Assuming an intra-cavity power of 3.2 kW, it will be possible to measure the Thomson signal down to an electron density of 3 x 10^{10} cm^{-3} at 1 eV. Figure 8 depicts the Thomson, Rayleigh equivalent background, and dark count signals expected for a T_e= 1 eV at a density of 3 x 10^{10} cm^{-3} (Fig. 8a) and 3 x 10^{12} cm^{-3} (Fig. 8b). The Rayleigh equivalent background is a means to model the elastically scatter laser light within the chamber. Low density measurements will require collection times of seconds, but if the intra-cavity power can be further increased via improved coupling or higher reflectivity mirrors the collection time can be significantly reduced. Additionally, using phase sensitive detection periodic phenomena such as the Hall effect thruster breathing mode can be studied. The multichannel scaler can be triggered off the discharge current to generate periodic data. At higher electron temperature the Thomson line shape broadens and would require a larger scan in wavelength to measure the shape. Further, there are xenon emission lines about the Thomson feature, but the lines are 7 nm or greater away from the line center (1064 nm) and the lines are narrow, which would reduce the spectral interference with the Thomson measurement.

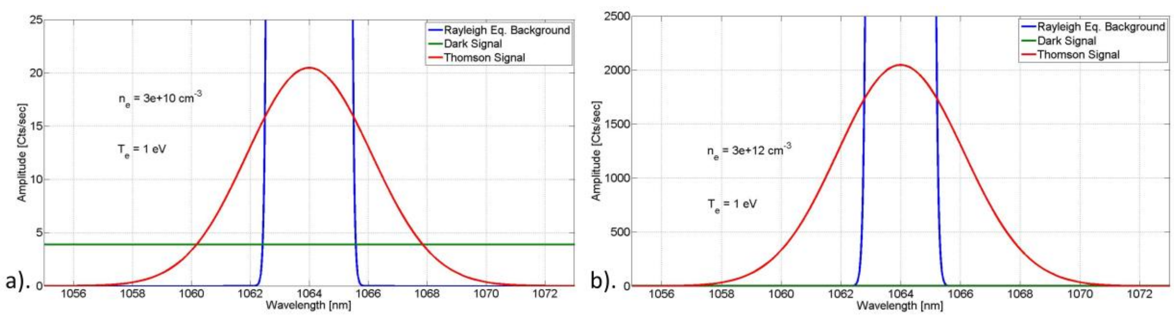

Figure 8. Scattering Spectra. *The simulated Thomson, Rayleigh equivalent back ground, and dark count rate are simulated for 1 eV xenon plasma at a density of a). n_e = 3 x 10^{10} cm^{-3} and b). n_e= 3 x 10^{12} cm^{-3}.*

V. Conclusion

The CETS diagnostic has progressed from a low-power proof of concept instrument to a high-power vacuum facility integrated system. The diagnostic has demonstrated high-quality measurements of rotational Raman and Rayleigh scattering on both the low- and high-power setups. An intra-cavity power of 3.2 kW and power build-up factor of 3300 has also been demonstrated. The ability to measure relatively weak scattering and to lock in the presence of plasma, albeit for short intervals of time, support the viability of the approach. System noise has been characterized as well as the available servo bandwidth and feedback options. With improved locking and cavity designs the system will be capable of intra-cavity powers in the range of 10-100 kW enabling measurements in EP devices at low plasma densities.

Acknowledgments

This work was supported by a NASA Space Technology Research Fellowship (NNX14AL42H) as well as by the NSF/DOE Partnership in Basic Plasma Science and Engineering (DE-SC0010519). A. J. Friss thanks the Colorado State University CEPPE lab, Plasma Controls, and Dr. John Williams for the use of an instant-start BaO hollow cathode and technical support regarding its operation.

References

[1] Mott-Smith, H. M., and Langmuir, I., "The theory of collectors in gaseous discharges," *Physical Review*, vol. 28, 1926, pp. 727–763.

[2] Haas, J. M., Gallimore, A. D., McFall, K., and Spanjers, G., "Development of a high-speed, reciprocating electrostatic probe system for Hall thruster interrogation," *Review of Scientific Instruments*, vol. 71, 2000, pp. 4131–4138.

[3] Hofer, R. R., and Gallimore, A. D., "Recent Results From Internal and Very-Near-Field Plasma Diagnostics of a High Specific Impulse Hall Thruster," 2003.

[4] Hutchinson, I. H., *Principles of Plasma Diagnostics*, Cambridge: Cambridge Univeristy Press, 2005.

[5] Muraoka, K., and Kono, A., "Laser Thomson scattering for low-temperature plasmas," *Journal of Physics D: Applied Physics*, vol. 44, Feb. 2011, p. 043001.

[6] Bowden, M. D., Goto, Y., Yanaga, H., Howarth, P. J. A., Uchino, K., and Muraoka, K., "A Thomson scattering diagnostic system for measurement of electron properties of processing plasmas," *Plasma Sources Science and Technology*, vol. 8, 1999, pp. 203–209.

[7] Washeleski, R. L., Meyer, E. J., and King, L. B., "Laser Thomson Scattering Measurements of Electron Temperature and Density in the Near-Field Plume of a Hall-Effect Thruster," *American Institute of Aeronautics and Astronautics*, 2012, pp. 1–17.

[8] Goebel, D., and Katz, I., *Fundamentals of electric propulsion: ion and Hall thrusters*, 2008.

[9] Cronrath, W., Bowden, M. D., Uchino, K., Muraoka, K., Muta, H., and Yoshida, M., "Spatial distributions of electron temperature and density in electron cyclotron resonance discharges," *Journal of Applied Physics*, vol. 81, 1997, pp. 2105–2113.

[10] Mansour ElSabbagh, M. a., Bowden, M. D., Uchino, K., and Muraoka, K., "Observations of bi-Maxwellian and single Maxwellian electron energy distribution functions in a capacitively coupled radio-frequency plasmas by laser Thomson scattering," *Applied Physics Letters*, vol. 78, 2001, p. 3187.

[11] ElSabbagh, M. A. M., Koyama, H., Bowden, M. D., Uchino, K., and Muraoka, K., "A Laser Thomson Scattering System for Low Density Glow Discharge Plasmas," vol. 40, 2001, pp. 1465–1466.

[12] Yamamoto, N., Tomita, K., Sugita, K., Kurita, T., Nakashima, H., and Uchino, K., "Measurement of xenon plasma properties in an ion thruster using laser Thomson scattering technique.," *The Review of scientific instruments*, vol. 83, Jul. 2012.

[13] Bowden, M. D., Tabata, R., Suanpoot, P., Uchino, K., Muraoka, K., and Noguchi, M., "Measurements of the electron energy distribution function in an Ar/CF[sub 4] inductively coupled plasma," *Journal of Applied Physics*, vol. 90, 2001, p. 2158.

[14] Yamamoto, N., Sugita, K., Kurita, T., Tomita, K., Uchino, K., and Nakashima, H., "Measurement of Plasma Property in an Ion Thruster using Laser Thomson Scattering Technique," *32nd International Electric Propulsion Conference*, 2011.

[15] Friss, A., Lee, B., Franka, I., and Yalin, A., "Cavity enhanced thomson scattering for diagnostics of weakly ionized discharges," *44th AIAA Plasmadynamics and Lasers Conference*, 2013.

[16] Friss, A., Lee, B., Franka, I., and Yalin, A. P., "Towards a Cavity Enhanced Thomson Scattering Diagnostic for Electric Propulsion Research," *IEPC-2013-351*, 2013, p. 351.

[17] Friss, A. J., Limbach, C., and Yalin, A. P., "Development of a Cavity Enhanced Thomson and Raman Scattering Diagnostic," *54th AIAA Aerospace Sciences Meeting*, 2016, pp. 1–10.

[18] Friss, A., and Yalin, A., "Further development of cavity enhanced thomson scattering for plasma thruster diagnostics," *53rd AIAA/SAE/ASEE Joint Propulsion Conference, 2017*, 2017.

[19] Black, E. D., "An introduction to Pound–Drever–Hall laser frequency stabilization," *American Journal of Physics*, vol. 69, 2001, p. 79.

[20] Kogelnik, H., and Li, T., "Laser beams and resonators," *Proceedings of the IEEE*, vol. 5, 1966, pp. 1550–1567.

[21] Donley, E. A., Heavner, T. P., Levi, F., Tataw, M. O., and Jefferts, S. R., "Double-pass acousto-optic modulator system," *Review of Scientific Instruments*, vol. 76, 2005, p. 063112.

[22] Friss, A. J., Limbach, C. M., and Yalin, A. P., "Cavity-enhanced rotational Raman scattering in gases using a 20 mW near-infrared fiber laser," *Optics Letters*, vol. 41, 2016, p. 3193.

[23] Miles, R. B., Lempert, W. R., and Forkey, J. N., "Laser Rayleigh scattering," *Measurement Science and Technology*, vol. 12, May 2001, pp. R33–R51.

[24] Lee, B. C., Yalin, A. P., and Gallimore, A., "Real-Time Boron Nitride Erosion Measurements of the HiVHAc Thruster via Cavity Ring-Down Spectroscopy," 2013, pp. 1–15.